



Organophosphorous pesticide removal from water by graphene-based materials – Only adsorption or something else as well?

VLADAN ANIĆEVIĆ¹, MARKO JELIĆ², ALEKSANDAR Z. JOVANOVIĆ³, NEBOJŠA POTKONJAK², IGOR A. PAŠTI^{3*}# and TAMARA D. LAZAREVIĆ PAŠTI²

¹Military Technical Institute (VTI), Ratka Resanovića 1, 11132 Belgrade, Serbia, ²Vinča Institute of Nuclear Sciences – National Institute of the Republic of Serbia, University of Belgrade, Mihajla Petrovića Alasa 12–14, Belgrade, Serbia and ³University of Belgrade – Faculty of Physical Chemistry, Studentski trg 12–16, 11158 Belgrade, Serbia

(Received 8 January, revised 11 February, accepted 12 February 2021)

Abstract: The extensive use of pesticides requires innovative approaches to remove these compounds from the environment. Carbon materials are traditionally used as adsorbents for removing pesticides, and the development of the new sorts of carbon materials allows more advanced approaches in environmental applications. Using density functional calculations, we have predicted chemical reaction between the S(O)=P moieties of the organophosphates with point defects in graphene – single vacancies, Stone–Wales defects and epoxy-groups. The reaction was confirmed using ultra high performance chromatography for two graphene oxide samples and dimethoate as a representative of organophosphates. The exact reaction mechanism is still elusive, but it is unambiguously confirmed that no selective oxidation of dimethoate to more toxic oxo-analog occurs. The presented results can help to develop novel systems for the irreversible conversion of organophosphates to non-toxic compounds, without using aggressive chemical agents or external physical factors like UV radiation.

Keywords: graphene; pesticide; removal; adsorption; chemical reaction.

INTRODUCTION

The growing world population caused enlarged food production, which, on the other hand, requires different strategies to boost the yield. One of the strategies is to use different pesticides to protect crops and increase the amounts of obtained plant products. Today, different classes of pesticides exist, differing by their action and level of sophistication. However, less developed countries still use some older families of pesticides, which can have a significant impact, not

* Corresponding author. E-mail: igor@ffh.bg.ac.rs

Serbian Chemical Society member.

<https://doi.org/10.2298/JSC210108012A>

only on their target species, but also on humans and the living world in general.¹ The mentioned fact particularly relates to the use of organophosphorus pesticides (OPs), which rely their action on the inhibition of acetylcholine-esterase (AChE).² This enzyme is present in mammals, and the extensive exposure to OPs can cause severe neurotoxic effects.³

To reduce the health and the environmental impact of OPs, there are different remediation strategies. These include either removing OPs *via* suitable substrates, or their degradation using chemical, physical or biological agents,^{4–8} some of them being potentially rather aggressive. The adsorption of OPs on different substrates requires high surface area adsorbents, which have to be environmentally friendly and affordable for large scale use. Among many possible candidates, the carbon materials seem to be perfect due to the (generally) large surface area, the ability to tune the surface chemistry and low costs.^{9–11} Typically, the activated carbons are used, but a fundamental understanding of OPs adsorption on carbon materials requires well-defined adsorbates, allowing one to resolve crucial factors in OPs adsorption on carbon materials.

Considering the facts stated above, graphene and graphene-based materials are excellent candidates, as model adsorbents for OPs removal. We have previously shown that different graphene-based materials display different adsorption properties towards the removing of OPs *via* adsorption from aqueous solutions.⁴ Depending on the type of OP (aromatic or aliphatic), the removal of OPs will be governed by the concentration of defects and surface functionalities in graphene-based materials and the existence of extended sp²-hybridized domains in the graphene basal plane.

The majority of our knowledge about the adsorption of OPs on carbon materials comes from experimental studies. However, theoretical analysis can provide us with valuable pieces of information as the model systems can be controlled at a high level. However, theoretical studies are rather scarce.¹² We believe that this is caused by the complexity of the systems and large sizes of OP molecules, making the direct electronic structure calculations heavy and time-consuming.

Nevertheless, we emphasize that the theoretical modelling can help us understand general trends, and certain approximations introduced in the model could allow us to perform the analysis, which could be very difficult, if not impossible, in the laboratory. In this contribution, we studied OPs adsorption on four different graphene model surfaces. As we have previously found that the S=P and O=P moieties of OPs dominate the adsorption on carbon materials, we simplify the models of OPs as S=PH₃ and O=PH₃. To control the electron density at S=P and O=P moieties, we replaced hydrogen atoms with highly electronegative fluorine atoms and consider S=PF₃ and O=PF₃ model OPs as well. In most cases, we found that the OPs adsorption is physical, but certain model molecules could also get chemically decomposed on the defective graphene surfaces. Chemical trans-

formations were also observed experimentally using UPLC analysis, while the preferential oxidation of thiophosphates into their highly toxic oxo-analogs was excluded by the direct evaluation of neurotoxicity of OP solution after the treatment with graphene oxide samples.

EXPERIMENTAL

Theoretical calculations

DFT calculations were done using QuantumESPRESSO code¹³ at the GGA level.¹⁴ The ultrasoft pseudopotentials were used, and the plane-wave basis set was expanded to 600 eV. The dispersion interactions were accounted for using the DFT-D3 approach of Grimme.¹⁵ The graphene surfaces were modelled in a 4×4 cell, originally containing 32 carbon atoms. The vacuum size was set to 20 Å to prevent the coupling of periodic images along the z-axis of the cell. First Brillouin zone was sampled using the 10×10×1 Monkhorst–Pack k-point set.¹⁶ The relaxation of all the atoms in the cell was allowed until the forces acting on atoms were below 0.01 eV Å⁻¹. Adsorption energies (E_{ads}) were calculated as:

$$E_{\text{ads}} = E_0(\text{OP+graphene}) - E_0(\text{graphene}) - E_0(\text{OP}) \quad (1)$$

where $E_0(\text{OP+graphene})$, $E_0(\text{graphene})$, and $E_0(\text{OP})$ stand for the total energies of: *i*) the graphene surface with adsorbed OP, *ii*) the clean graphene surface and *iii*) the isolate OP model molecule, respectively.

Materials

For the present study, we chose two commercial graphene oxide (GO) materials and dimethoate (DMT) as a representative of OPs. This combination of OP and adsorbents was justified because GO is not a very good adsorbent for removing DMT but possesses many different surface functional groups and defects. Hence, the possible chemical conversion of DMT *via* reactions with the surface functional groups is easier to observe, when compared to the situation when extremely effective adsorbents are used. Namely, in that scenario, all DMT would be adsorbed, and it would not be possible to see the reaction products. We specifically used GRAPHENEA GO,¹⁷ denoted hereafter as GNA GO and Graphene Supermarket GO¹⁸ denoted further as SM GO. GNA GO has 49–56 % of carbon and 41–50 % oxygen, with small amounts of hydrogen, nitrogen and sulphur. It also has a high concentration of epoxy groups, as confirmed by the manufacturer using XPS. SM GO has a higher carbon-to-oxygen ratio (79 to 20 %).

Adsorption measurements

The investigated adsorbents were dispersed in double-distilled water, and the desired amount of DMT stock solution (Pestanal, Sigma Aldrich, Denmark) was added to provide the targeted concentration of the adsorbent and DMT. The vessel containing the adsorbent+DMT mixture was then placed on a laboratory shaker (Orbital Shaker-Incubator ES-20, Grant-Bio) and left for 21 h at 25 °C to ensure reaching the equilibrium. After the equilibrium was reached, the mixture was centrifuged for 10 min at 14500 rpm, and the supernatant was filtered through the nylon filter membrane. The concentration of DMT after adsorption (C_{eq}) was determined using UPLC analysis. The control experiments were performed identically, but without the carbon adsorbents, and confirmed that there is no DMT degradation within the timeframes of the described experiments. From the described batch adsorption measurements, we calculated uptake for the investigated DMT on all the studied adsorbents, varying the

adsorbent dose and for fixed DMT concentration ($C_0 = 5 \times 10^{-4}$ M). The removal was calculated as:

$$\text{Removal} = 100(C_0 - C_{\text{eq}})/C_0 = 100C_{\text{ads}}/C_0 \quad (2)$$

UPLC analysis

The Waters ACQUITY ultra performance liquid chromatography (UPLC) system coupled with a tunable UV detector controlled by the Empower software was used. The chromatographic separations were run on an ACQUITY UPLC™ BEH C₁₈ column, with the dimensions 1.7 µm, 100 mm × 2.1 mm (Waters). The DMT analysis was done under isocratic conditions, with the mobile phase consisting of acetonitrile (phase A, 20 vol.%) and 20 vol.% acetonitrile in water (phase B, 80 vol.%). The eluent flow rate was 0.25 mL min⁻¹, and the injection volume was 10 µL. The optical detection was done using a photodiode array detector. Under the described conditions, the retention time of DMT was 3.02±0.05 min.

Neurotoxicity measurements

Regarding their (neuro)toxicity, the physiological effects of treated DMT solutions were tested using AChE inhibition measurements. AChE activity was assayed according to Ellman's procedure.¹⁹ The *in vitro* experiments were performed by the exposure of 2.5 IU commercially purified AChE from electric eel to the OP solutions obtained in the adsorption experiments (batch adsorption or filtration) at 37 °C in 50 mM PB pH 8.0 (final volume 0.650 mL). The enzymatic reaction was started by the addition of acetylcholine-iodide (AChI) in combination with DTNB as a chromogenic reagent and allowed to proceed for 8 min until stopped by 10 % sodium dodecyl sulfate (SDS). The enzymatic reaction product, thiocholine, reacts with DTNB and forms 5-thio-2-nitrobenzoate, whose optical adsorption was measured at 412 nm. It should be noted that in these measurements, the enzyme concentration was constant and set to give an optimal spectrophotometric signal. Physiological effects were quantified as AChE inhibition given as:

$$\text{AChE inhibition} = 100 \frac{A_0 - A}{A_0} \quad (3)$$

where A_0 and A stand for the AChE activity in the absence of OP and the one measured after the exposure to a given OP.

RESULTS AND DISCUSSION

Model OPs

All the studied (O)SPH₃(F₃) have C_{3v} symmetry. When hydrogen atoms are replaced with the electron-withdrawing fluorine atoms, the O=P and S=P bonds were contracted. O=P bond, the length is reduced from 1.49 to 1.46 Å, while for the S=P bond, the length reduces from 1.94 to 1.88 Å. These results demonstrate that the idea to control the electron density at the O=P and S=P moieties by changing hydrogen with fluorine was correct.

Model graphene-based surfaces

To investigate the effects of different graphene-based surfaces on the adsorption processes of model OPs, we considered four different surfaces. These are pristine graphene surface, graphene surface with a single vacancy, graphene surface with Stone–Wales (SW) defect and graphene surface with one epoxy

group.²⁰ We do not describe these surfaces in detail, but here are provided their densities of states (DOS) and their optimized structures (Fig. 1).

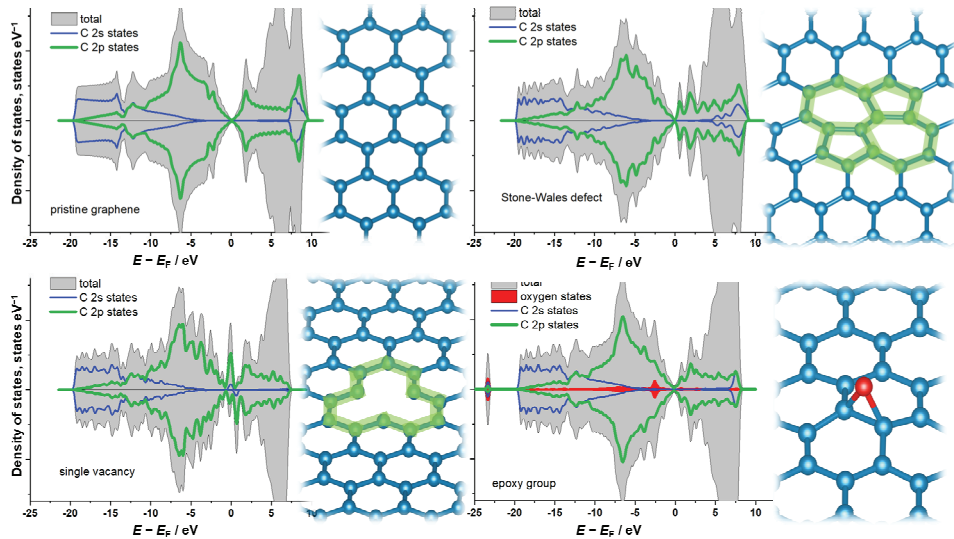


Fig. 1. Densities of states (DOS) and the optimized structures of considered model graphene surfaces. For graphene with the single vacancy and Stone–Wales (SW) defect, the defects are indicated in the corresponding structures.

The introduction of considered defects causes the large electronic structure disruptions, when compared to the electronic structure of pristine graphene. Graphene with a single vacancy remains flat, like pristine graphene. However, the dangling bonds are formed upon removing one C atom, and the corresponding states are located around the Fermi level.

There are pronounced DOS changes around the Fermi level for the SW defects, as the formation of the SW defect is preceded by the rehybridization of carbon atoms and the local bending. This local bending expands further to the entire basal plane for the studied concentration of SW defects. The addition of the epoxy group on the graphene basal plane causes sp^2 to sp^3 rehybridization of the carbon atoms bonded to oxygen. Hence, in this case, too, there is a local deformation of the basal plane. While one cannot expect that pristine graphene should show significant chemical reactivity, the introduction of defects can change the situation dramatically.

Interaction of model OPs with model graphene-based surfaces

The next step performed was the analysis of model OPs interactions with the described graphene-based surfaces. Molecules were soft-landed on the surfaces, and the systems were completely relaxed without any restrictions during the structural optimization. In line with our previous experimental findings,⁹ we con-

cluded that the interaction is *via* S=P or O=P moiety. Moreover, the calculated adsorption energies indicated physisorption, when no chemical reaction between model OPs and the studied adsorbates occurs. The results are summarized in Table I.

TABLE I. Calculated adsorption energies (eV) for model OPs on four considered graphene-based surfaces. When “reaction” is stated, no structures with intact model OPs were observed upon the relaxation

Substrate	Surface			
	S=PH ₃	S=PF ₃	O=PH ₃	O=PF ₃
Pristine graphene	-0.18	-0.14	-0.16	-0.15
Graphene with Stone–Wales defect	-0.26	-0.19	-0.28	-0.19
Graphene with a single vacancy	Reaction	Reaction	-0.27	-0.22
Epoxy graphene	Reaction	Reaction	Reaction	Reaction

These few numbers presented in Table I tell a story of importance. As expected, the pristine graphene interacts weakly with model OPs. However, when the SW defect has been introduced, the interactions, which are still weak, become stronger. As for pristine graphene, the F-substituted molecules interact weaker with the SW graphene surface.

When the model OPs interacted with the graphene with the single vacancy, we observed that tio-forms always reacted with the graphene surface. However, for oxo-forms, we identified the cases where model OPs were intact after the adsorption. The adsorption energies calculated for these cases were similar to that in the case of SW graphene. This result showed that the oxo-forms were more stable than tio-forms, which is in accordance with our previous results about DMT oxidation and the product of the oxidation – omethoate, is more stable and more persistent to chemical modifications than its parental tio-form DMT. Finally, all the considered model OPs undergo chemical transformations when interacted with epoxy-group on graphene.

Physisorption of model OPs is clearly seen in DOS plots of studied systems where no model OPs react. Such a situation is shown for OPH₃ and OPF₃ on the SW graphene surface in Fig. 2.

The electronic states of OPH₃ and OPF₃ simply add up to the electronic states of the surface, which is almost unchanged when compared to the DOS of the clean surface (Fig. 1). Also, by comparing the DOSes presented in Fig. 2, one can see that the states of carbon atoms are almost identical for OPH₃ and OPF₃ adsorbates.

Except for the pristine graphene surface, some chemical reactions between the model OPs and the defects in the surfaces were observed in all the other cases, in addition to the physisorption events reported in Table I. This will not be described in many details, as it is not certain that all these reactions might not occur with a real OP molecule due to steric hindrances. However, the general

conclusions follow. For the epoxy graphene surfaces, the O atom from the epoxy function always reacts with model OPs. As a rule, this process is followed by incorporating O, S or P molecules into the graphene lattice, with the significant reordering of the hexagonal carbon network. For the SW graphene and the graphene with a single vacancy, these topological defects are reactive sites. The O, S and P atoms of the model OPs incorporate easily into the graphene lattice, and the result is the graphene doped with one of these heteroatoms or (S,P)-co-doped graphene. Such a scenario is presented in Fig. 3, where, upon the landing of SPF_3 on the SW graphene surface, both S and P are incorporated into the SW lattice site. The states of S and P get fully hybridized with the states of carbon atoms. As a side note, this seems like a rather effective way to dope the graphene lattice with S and P, which opens many possibilities for using such doped graphene.

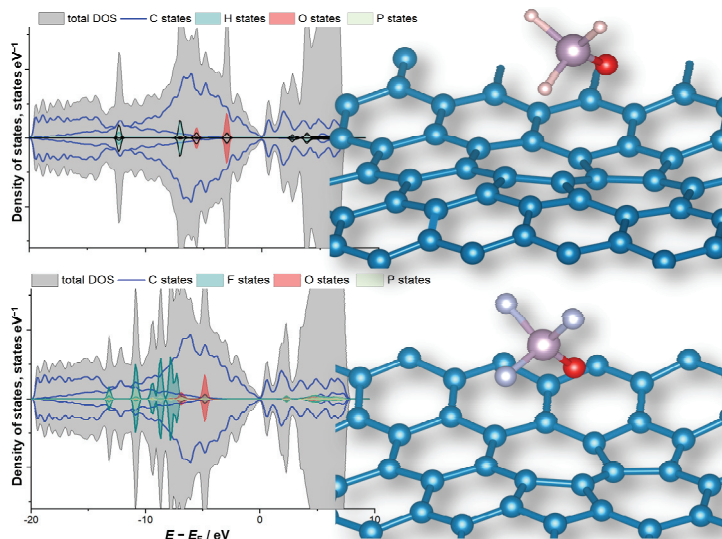


Fig. 2. Densities of states (DOS) and the optimized structures of model OPs interacting with the SW graphene surfaces.

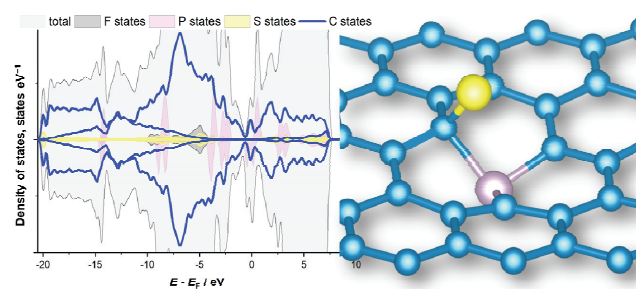


Fig. 3. Densities of states (DOS) and the optimized structure of SPF_3 upon the reaction with the SW graphene surface.

It is emphasized that the observed chemical reactions are spontaneous and, as a rule, disrupt the O=P or S=P moiety, which is directly responsible for the neurotoxicity of OPs.

Experimental results – UPLC analysis and neurotoxicity

To investigate the possible chemical reactions between OPs and graphene-based materials, we have performed a series of batch adsorption experiments using DMT and two commercial GO materials. The choice of GO as an adsorbent was explained previously. Upon the detailed analysis of UPLC chromatograms, we have identified one prominent signal that depends on the adsorbent mass (Fig. 4). This signal is located at a low retention time ($RT = 0.877$ min) and is well separated from the main DMT peak that appears at $RT = 3.02$ min. The signal at $RT = 0.877$ min is not present for the pure DMT solution and is not seen for the filtrate of pure GO adsorbents, which we have used as a background. The time evolution of this signal during the extended exposure to adsorbents is not very obvious, but it is visible. Moreover, there are slight variations in the retention time of the two chromatographic peaks. We suspect that the observed time variation can be understood as a balance between the chemical reaction giving the product with this specific signal in UPLC and its adsorption on GO, as well as the formation of more complex adducts.

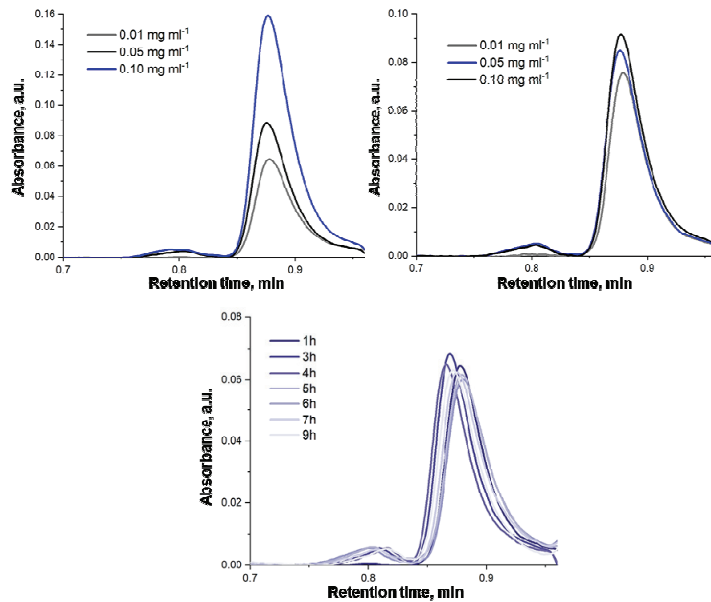


Fig. 4. UPLC chromatograms of DMT solution upon the batch adsorption experiment using SM GO (top left) and GNA GO (top right) for different masses of adsorbents. In the bottom row, the time evolution of the signal is presented for extended batch adsorption experiments using SM GO and DMT. The concentration of DMT was 5×10^{-4} mol dm $^{-3}$.

The observed signal is further analyzed, and the UV–Vis spectra were extracted (Fig. 5). This new signal shows broad adsorption, with the adsorption maximum at 199.2 nm. Contrary to that, a rather sharp absorption of DMT maximum is seen at 193.8 nm.

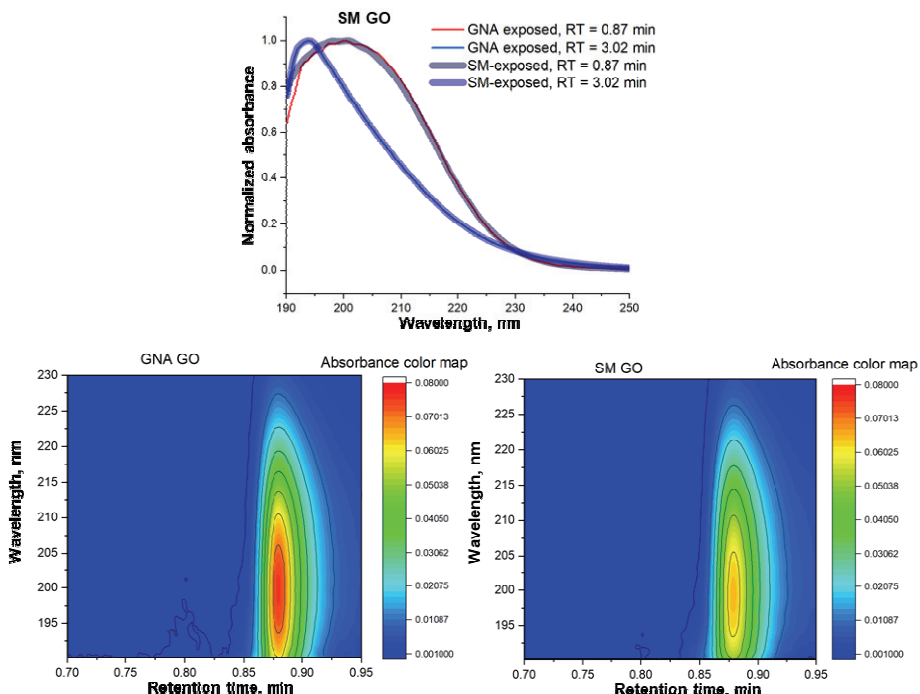


Fig. 5. Normalized UV spectra of the fraction corresponding to the retention time of 0.87 min and the UV spectra of DMT ($RT = 3.02$ min) upon the batch adsorption experiments using DMT ($C = 5 \times 10^{-4}$ mol dm^{-3}) and the concentration GO materials amounting to 0.01 mg ml^{-1} (upper row). In the bottom row, photodiode array signals (PDA) *versus* the retention time are provided for both GO used.

The only possible way to determine the exact mechanism of the DMT decomposition *via* GO substrates is the use of mass spectrometry coupled with UPLC. However, for the time being, this demanding task is left aside. Namely, we suspect that for other OPs one could expect different reaction mechanisms depending on the complexity of a given molecule. DMT is a rather simple aliphatic molecule, so deriving specific conclusions built up based on its case is risky. However, our main goal here was to communicate the chemical conversion of DMT with graphene oxide. Moreover, based on DFT calculation, we expected that the S=P moiety of OP molecules take part in chemical conversion and that this part of the molecule gets degraded. Hence, this reaction should reduce the

toxicity of the DMT solution after the treatment with a GO sample, being in favour for the remediation of OPs.

It is noted that the amount of chemically converted DMT is rather small, so the main removal mechanism could still be adsorption. The relatively low efficiency of GO materials as adsorbents for DMT is discernible from the data presented in Table II. The removal is characterized by equilibrium, with up to 10 % of DMT being adsorbed/reacted on GO materials. While the performed UPLC analysis showed no DMT conversion to its oxo-analog, we have performed an additional check using the AChE inhibition measurements. The reduction of AChE inhibition is a joint effect of adsorption (which is highly dominant) and chemical degradation of DMT caused by GO samples as adsorbents. In all the cases, the reduced AChE inhibition after the batch adsorption measurements was confirmed, so DMT-oxon (omethoate) formation can be securely excluded. Namely, if only a small fraction of DMT is converted to oxon, the AChE inhibition would increase as the oxon is approximately 1000 times more toxic than DMT.⁹

TABLE II. The calculated equilibrium concentration (C_{eq}) and DMT uptakes for three different DMT concentrations in the batch adsorption experiments using SM GO and GNA GO as adsorbent. AChE inhibition is evaluated for the filtrates after the experiments. The uncertainty of reported results is within 5 %

DMT concentration, mol dm ⁻³		Adsorbent C_{eq} / 10 ⁻⁴ mol dm ⁻³	Removal, %	AChE inhibition, %
10^{-3}	None	10.0	—	46
	SM GO	9.52	4.81	28
	GNA GO	9.59	4.1	29
10^{-4}	None	1.00	/	12
	SM GO	0.920	8.0	7
	GNA GO	0.942	5.8	8
10^{-5}	None	0.100	—	6
	SM GO	0.0908	9.2	0
	GNA GO	0.0889	11.1	0

CONCLUSION

Based on the DFT calculations of the interactions of different graphene-based surfaces and model organophosphorus molecules, a chemical reaction between point defects in graphene basal plane (single vacancy, Stone–Wales defect and epoxy group) and the S(O)=P moieties of organophosphorus compounds is expected. Using UPLC analysis, this reaction is confirmed for two commercial graphene oxide samples and for DMT as a representative of organophosphorous pesticides. While DMT adsorption is still a dominant mechanism of the pesticide removal from aqueous solutions on studied GO materials, although very small, this reaction also contributes to the reduction of neurotoxicity of the graphene oxide-treated samples. The presented results could lead to the develop-

ment of novel systems for the irreversible conversion of organophosphates to non-toxic compounds.

Acknowledgement. Authors acknowledge the financial support provided by the Serbian Ministry of Education, Science and Technological Development through the institutional funding of "VINČA" Institute of Nuclear Sciences – National Institute of the Republic of Serbia and the University of Belgrade – Faculty of Physical Chemistry.

И З В О Д

УКЛАЊАЊЕ ОРГАНОФОСФОРНИХ ПЕСТИЦИДА ИЗ ВОДЕ КОРИШЋЕЊЕМ МАТЕРИЈАЛА НА БАЗИ ГРАФЕНА – САМО АДСОРЦИЈА ИЛИ ЈОШ НЕШТО?

ВЛАДАН АНИЋИЕВИЋ¹, МАРКО ЈЕЛИЋ², АЛЕКСАНДАР З. ЈОВАНОВИЋ³, НЕБОЈША ПОТКОЊАК²,
ИГОР А. ПАШТИ¹ и ТАМАРА Д. ЛАЗАРЕВИЋ-ПАШТИ²

¹Војно технички институут (ВТИ), Радика Ресановића 1, 11132 Београд, ²Институут за нуклеарне науке Винча – Национални институут означаја за Републику Србију, Универзитет у Београду, Михајла Петровића Аласа 12–14, Београд и ³Универзитет у Београду – Факултет за физичку хемију,
Студентски тор 12–16, 11158 Београд

Широка употреба пестицида захтева иновативне приступе уклањању ових једињења из животне средине. Угљенични материјали се традиционално користе као адсорбенти за уклањање пестицида, а развој нових врста угљеничних материјала омогућава напредније приступе у њиховој примени у животној средини. Користећи прорачуне базиране на теорији функционала густине, предвиђена је хемијска реакција између S(O)=P група органосфосфата са тачкастим дефектима у графену – појединачним ваканцијама, Стоне–Вејлс (Stone–Wales) дефеката и епоксидног група. Реакција је потврђена хроматографијом ултра високих перформанси за два узорка графен-оксида и диметоата као представника органофосфорних пестицида. Тачан реакциони механизам је још увек неразјашњен, али је недвосмислено потврђено да се не јавља селективна оксидација диметоата у токсичнији оксо-аналог. Презентовани резултати могу помоћи у развоју нових система за иреверзибилну конверзију органофосфорних пестицида у нетоксична једињења без употребе агресивних хемијских агенаса, или спољних физичких фактора попут UV зрачења.

(Примљено 8. јануара, ревидирано 11. фебруара, прихваћено 12. фебруара 2021)

REFERENCES

1. J. E. Casida, G. B. Quistad, *Chem. Res. Toxicol.* **17** (2004) 983 (<https://doi.org/10.1021/tx0499259>)
2. M. B. Colovic, D. Z. Krstic, T. D. Lazarevic-Pasti, A. M. Bondzic, V. M. Vasic, *Curr. Neuropharmacol.* **11** (2013) 315 (<https://doi.org/10.2174/1570159X11311030006>)
3. T. Lazarevic-Pasti, A. Leskovac, T. Momic, S. Petrovic, V. Vasic, *Curr. Med. Chem.* **24** (2017) 3283 (<https://doi.org/10.2174/0929867324666170705123509>)
4. T. Lazarević-Pasti, V. Anićijević, M. Baljozović, D. Vasić Anićijević, S. Gutić, V. Vasić, N. V. Skorodumova, I. A. Pašti, *Environ. Sci.: Nano* **5** (2018) 1482 (<https://doi.org/10.1039/C8EN00171E>)
5. T. Mitrović, S. Lazović, B. Nastasijević, I. A. Pašti, V. Vasić, T. Lazarević-Pasti, *J. Environ. Manage.* **246** (2019) 63 (<https://doi.org/10.1016/j.jenvman.2019.05.143>)
6. M. I. Badawy, M. Y. Ghaly, T. A. Gad-Allah, *Desalination* **194** (2006) 166 (<https://doi.org/10.1016/j.desal.2005.09.027>)

7. T. Matsushita, A. Morimoto, T. Kuriyama, E. Matsumoto, Y. Matsui, N. Shirasaki, T. Kondo, H. Takanashi, T. Kameya, *Water Res.* **138** (2018) 67 (<https://doi.org/10.1016/j.watres.2018.01.028>)
8. Y. Samet, L. Agengui, R. Abdelhedi, *J. Electroanal. Chem.* **650** (2010) 152 (<https://doi.org/10.1016/j.jelechem.2010.08.008>)
9. T. D. Lazarević-Pašti, I. A. Pašti, B. Jokić, B. M. Babić, V. M. Vasić, *RSC Adv.* **6** (2016) 62128 (<https://doi.org/10.1039/C6RA06736K>)
10. M. Valickova, J. Dercó, K. Simovicova, *Acta Chim. Slovaca* **6** (2013) 25 (<https://doi.org/10.2478/acs-2013-0005>)
11. M. Vukčević, A. Kalijadis, B. Babić, Z. Laušević, M. Laušević, *J. Serb. Chem. Soc.* **78** (2013) 1617 (<https://doi.org/10.2298/JSC131227006V>)
12. S. M. Maliekal, T. S. Sreeprasad, D. Krishnan, S. Kouser, A. Kumar Mishra, U. V. Waghmare, T. Pradeep, *Small* **9** (2013) 273 (<https://doi.org/10.1002/smll.201201125>)
13. P. Giannozzi, S. Baroni, N. Bonini, M. Calandra, R. Car, C. Cavazzoni, D. Ceresoli, G. L. Chiarotti, M. Cococcioni, I. Dabo, A. Dal Corso, S. de Gironcoli, S. Fabris, G. Fratesi, R. Gebauer, U. Gerstmann, C. Gougaussis, A. Kokalj, M. Lazzeri, L. Martin-Samos, N. Marzari, F. Mauri, R. Mazzarello, S. Paolini, A. Pasquarello, L. Paulatto, C. Sbraccia, S. Scandolo, G. Sclauzero, A. P. Seitsonen, A. Smogunov, P. Umari, R. M. Wentzcovitch, *J. Phys. Condens. Matter* **21** (2009) 395502 (<https://doi.org/10.1088/0953-8984/21/39/395502>)
14. J. P. Perdew, K. Burke, M. Ernzerhof, *Phys. Rev. Lett.* **77** (1996) 3865 (<https://doi.org/10.1103/physrevlett.77.3865>)
15. S. Grimme, J. Antony, S. Ehrlich, H. Krieg, *J. Chem. Phys.* **132** (2010) 154104 (<https://doi.org/10.1063/1.3382344>)
16. H. J. Monkhorst, J. D. Pack, *Phys. Rev., B* **13** (1976) 5188 (<https://doi.org/10.1103/PhysRevB.13.5188>)
17. https://cdn.shopify.com/s/files/1/0191/2296/files/Graphenea_GO_4mgmL_Datasheet_201905.pdf?22 (accessed on January 3, 2021)
18. <http://graphene-supermarket.com/images/P/Graphene%20Oxide-Data-Sheet-Graphene-Supermarket.pdf> (accessed on January 3, 2021)
19. G. L. Ellman, K. D. Courtney, V. Andres jr., R. M. Featherstone, *Biochem. Pharmacol.* **7** (1961) 88 ([https://doi.org/10.1016/0006-2952\(61\)90145-9](https://doi.org/10.1016/0006-2952(61)90145-9))
20. G. Yang, L. Li, W. Bun Lee, M. Cheung Ng, *Engin. Struct. Mater.* **19** (2018) 613 (<https://doi.org/10.1080/14686996.2018.1494493>).